ACS OMEGA

Article

Cite This: ACS Omega 2019, 4, 20756−20761

http://pubs.acs.org/journal/acsodf

Solar-Blind UV Photodetector Based on Atomic Layer-Deposited Cu_2O and Nanomembrane β-Ga_2O_3 pn Oxide Heterojunction

Hagyoul Bae,[†,‡] Adam Charnas,[†,‡] Xing Sun,[§] Jinhyun Noh,[†,‡] Mengwei Si,[†,‡] Wonil Chung,[†,‡] Gang Qiu,[†,‡] Xiao Lyu,[†,‡] Sami Alghamdi,[†,‡] Haiyan Wang,[§] Dmitry Zemlyanov,[‡] and Peide D. Ye*[,†,‡]

[†]School of Electrical and Computer Engineering, [‡]Birck Nanotechnology Center, [§]School of Materials Engineering, Purdue University, West Lafayette, Indiana 47907, United States

Supporting Information

ABSTRACT: Herein, we present a solar-blind ultraviolet photodetector realized using atomic layer-deposited p-type cuprous oxide (Cu_2O) underneath a mechanically exfoliated n-type β-gallium oxide (β-Ga_2O_3) nanomembrane. The atomic layer deposition process of the Cu_2O film applies bis(*N*,*N*′-di-secbutylacetamidinato)dicopper(I) [Cu(^{5}Bu-Me-amd)]$_2$ as a novel Cu precursor and water vapor as an oxidant. The exfoliated β-Ga_2O_3 nanomembrane was transferred to the top of the Cu_2O layer surface to realize a unique oxide pn heterojunction, which is not easy to realize by conventional oxide epitaxy techniques. The current−voltage (*I*−*V*) characteristics of the fabricated pn heterojunction diode show the typical rectifying behavior. The fabricated Cu_2O/β-Ga_2O_3 photodetector achieves sensitive detection of current at the picoampere scale in the reverse mode. This work provides a new approach to integrate all oxide heterojunctions using membrane transfer and bonding techniques, which goes beyond the limitation of conventional heteroepitaxy.

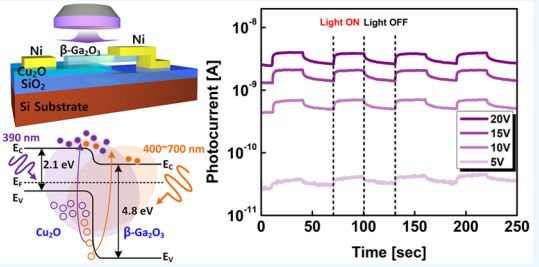

INTRODUCTION

Solar-blind ultraviolet (UV) photodetectors have been actively investigated recently because of their variety of potential applications in the fields of military surveillance, biological/chemical analyses, astronomical observations, and optical communications.[1−3] Recently, photonic devices based on various materials have been widely investigated due to their intrinsic properties, including high transparency and excellent sensitivity.[4−7] Among the oxide-based materials, especially, cuprous oxide (Cu_2O) is a natural p-type semiconductor with a bandgap of 2.1 eV[8] that can be photoexcited in the UV/visible spectral region.[9] Moreover, it exhibits unique properties such as high absorption efficiency, non-toxicity, abundant availability, and low production costs.[10−12] The atomic layer deposition (ALD) process is particularly suited for oxide materials growth with a variety of applications in high-k gate dielectric and highly scaled dynamic random access memory capacitor integration because of its conformal step coverage and atomic layer thin thickness control.[13] Although many studies of the ALD growth of metallic Cu have been reported, only a few studies related to ALD grown Cu_2O have been performed.[14−16] As determined from their bandgaps, binary compound semiconductors including GaN, SiC, and ZnO are suitable for developing visible-blind UV detectors, which are required for higher responsivity in the UV range compared to lower energy ranges. To meet the criteria of a solar-blind photodetector with a cutoff wavelength below 280 nm, alloy engineering is used to tune the bandgap as high as 4.42 eV to eliminate the longer wavelength. For instance, AlGaN[17] and MgZnO[18] wide bandgap (WBG) ternary semiconductor alloys were used to develop solar-blind photodetectors, achieving rapid progress for the development of high-performance avalanche solar-blind photodetectors with improved photoresponsivity and response speed. However, these materials required a high growth temperature above 1350 °C. The phase segregation from wurtzite to rock salt structure[19] results in the degradation of detecting performance. Alternatively, ultraWBG (UWBG) β-Ga_2O_3 semiconductors have been actively developed for UV-transmitting optoelectronic applications,[20−23] owing to their UWBG of 4.8−4.9 eV,[24,25] the availability of large-size β-Ga_2O_3 bulk single crystals,[26] and homoepitaxial growth of high crystalline quality epitaxial layers with the possibility for doping and bandgap engineering.[27] In particular, the exfoliated β-Ga_2O_3 nanomembrane transfer technique offers the opportunity to demonstrate some of the prototype device concepts, which are usually difficult to realize using conventional material growth techniques.

Herein, we demonstrate a heterojunction photodetector by integrating ALD-grown p-type Cu_2O with an exfoliated β-Ga_2O_3 nanomembrane to form a suspended pn heterojunction structure. The ALD process can be applied for photovoltaic applications, in particular for depositing ultrathin layers at

Received: September 24, 2019
Accepted: November 13, 2019
Published: November 22, 2019

DOI: 10.1021/acsomega.9b03149
ACS Omega 2019, 4, 20756−20761

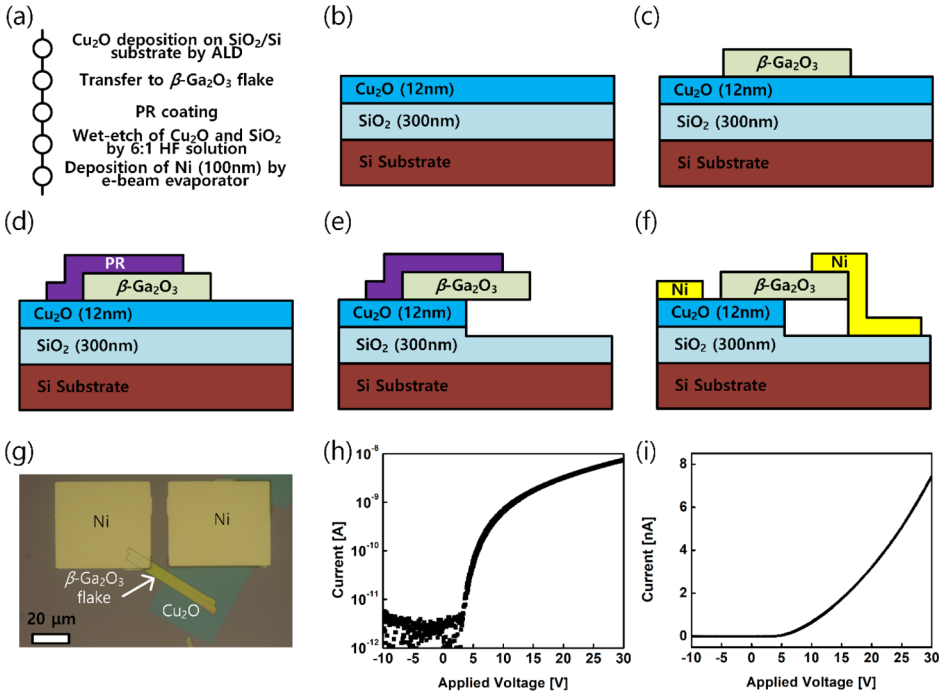

Figure 1. Schematic illustration of the fabrication procedure of the Cu_2O/β-Ga_2O_3 photodetector and typical current voltage (I–V) characteristics. (a) Simplified process flow for the fabricated device. (b–f) Show schematics of the proposed atomic layer deposited p-type Cu_2O/suspended n-type β-Ga_2O_3 heterojunction pn diode. (g) Optical photograph showing the fabricated photodetector. Measured I–V characteristic curves with (h) log (I)–linear (V) and (i) linear (I)–linear (V) scale under the dark state.

relatively low temperatures. We report the fabrication and characterization of a solar-blind UV photodetector based on the Cu_2O/β-Ga_2O_3 heterojunction with low dark and photonic currents for highly sensitive photodetector applications.

RESULTS AND DISCUSSION

Figure 1 shows the schematic illustration of the procedure used for fabricating the Cu_2O/β-Ga_2O_3 pn heterojunction photodetector with a suspended structure. A representative fabrication process is listed in Figure 1a. During the first fabrication step, a Cu_2O thin film was deposited on the oxide (270 nm SiO_2) of a p + Si wafer via ALD, as shown in Figure 1b. ALD is one of the most effective oxide growth techniques for producing ultrathin films at atomic layer accuracy. A single ALD cycle consists of Cu deposition and oxidation, as shown in Table S1 of the Supporting Information. In this study, bis(*N*,*N*′-di-*sec*-butylacetamidinato)dicopper(I) [Cu(^{s}Bu-Me-amd)]$_2$ was used as a novel Cu precursor. The structural formula of the Cu precursor is presented in Figure S1 of the Supporting Information. The ALD process for copper deposition features complementarity and self-limitation related to the surface reactions. The former feature involves two reactants for preparation of the surface for its reaction with the other vapor, allowing the deposition cycles to be repeated. In addition, the latter feature contributes to the very conformable uniform thickness even on nonuniform surface structures.[28] For a stable supply, the temperature of the canisters for the Cu precursor and H_2O was maintained constant at 130 and 30 °C, respectively. In a single thermal ALD Cu_2O cycle, the optimized process consists of a Cu-precursor pulse for 30 ms with a 100 sccm N_2 flow, a purge pulse of 11 s with 100 sccm of N_2 flow, a water pulse for 60 ms with 100 sccm N_2 flow, and a purge pulse of 11 s with 100 sccm of N_2 flow. During the ALD processes, the substrate temperature was maintained at the optimized growth temperature of 180 °C (Figure S2 in the Supporting Information) and the observed growth rate was ∼0.002 nm/cycle (Figure S3 in the Supporting Information). To improve the ALD growth rate and the film conductivity, plasma-enhanced ALD process with O_3 will be introduced in the near future. In the next step, the thin β-Ga_2O_3 nanomembrane was mechanically exfoliated from the bulk β-Ga_2O_3 substrate cleavage and transferred to the top of the Cu_2O layer on the SiO_2/Si substrate, as shown in Figure 1c. β-Ga_2O_3 nanomembrane is n-type with a Sn-doping concentration of 2.7×10^{18} cm^{-3}. The AZ1518 positive photoresist (PR) with a thickness of 1.8 μm was coated on the wafer, as shown in Figure 1d. To form two metal contacts on both the p-type Cu_2O film and n-type β-Ga_2O_3 flake, Cu_2O and SiO_2 layers were etched using a 6:1 HF solution for 60 min, as shown in Figure 1e. The PR acts as a hardmask to protect the Cu_2O film underneath the PR, while Cu_2O and SiO_2 were etched simultaneously. As shown in Figure 1g, two 100 nm Ni electrodes were deposited on the p-type Cu_2O film and n-type β-Ga_2O_3 nanomembrane. Figure 1g shows an optical image of the fabricated device with a 250 nm thick β-Ga_2O_3 flake including a 12 nm Cu_2O film and Ni electrodes. The contact properties with various metals on the Cu_2O film were studied and are summarized in Figure S4 of the Supporting Information. Figure 1h,i shows the current–voltage (I–V) characteristics of the fabricated device. The measured I–V curve of the Cu_2O/β-Ga_2O_3 pn heterojunction presents typical rectifying characteristics as a well-defined diode. The on-current was limited by both contact resistance and interface quality between the two heterogeneous oxide materials. Although the rectifying characteristics resemble the basic function of a pn heterojunction diode, further process optimization is needed to reduce the surface roughness, interface quality, the conductivity of the Cu_2O film, and its

DOI: 10.1021/acsomega.9b03149
ACS Omega 2019, 4, 20756−20761

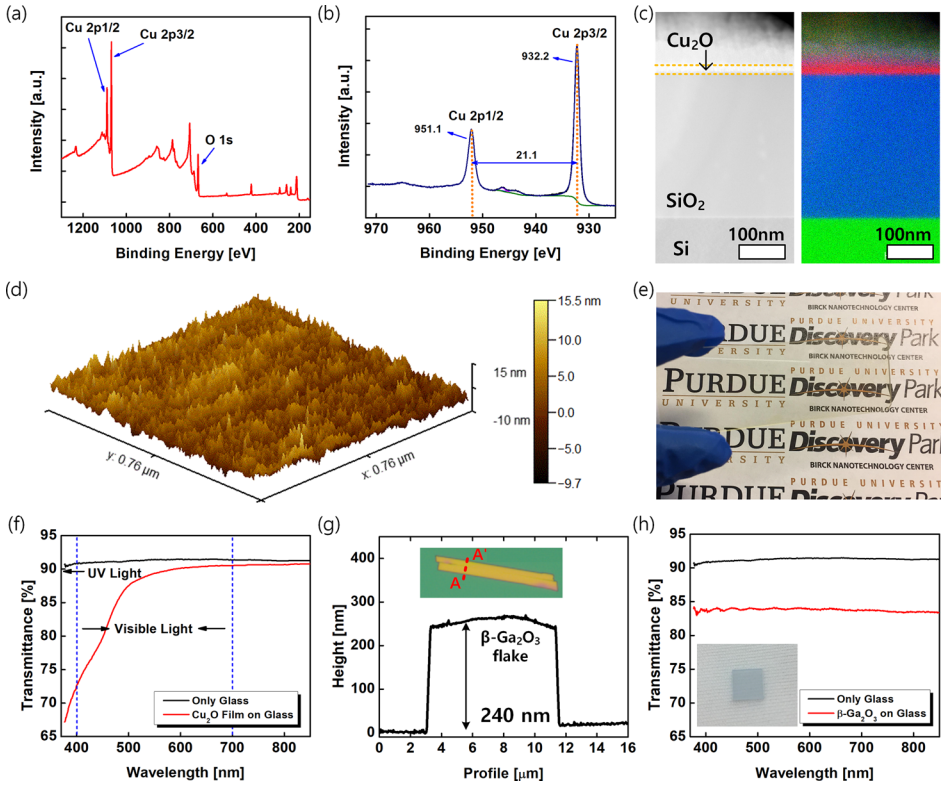

Figure 2. (a) Representative high-resolution XPS spectra analysis of the atomic layer deposited Cu_2O film based on bis(*N*,*N*′-di-*sec*-butylacetamidinato)dicopper(I) as a new precursor. (b) Cu $2p_{3/2}$ and Cu $2p_{1/2}$ peaks for Cu_2O film. (c) STEM and EDS mapping images of each layer (Cu_2O, SiO_2, Si substrate) (d) AFM image of the surface morphology for ALD-grown Cu_2O thin film. (e) Image showing the transparency of the ALD-grown Cu_2O film with a thickness of 12 nm. (f) Measured transmittance of the ALD-grown Cu_2O film at various wavelengths. (g) Measured height of the exfoliation-type β-Ga_2O_3 flake. (h) Measured transmittance of the exfoliated β-Ga_2O_3 flake at various wavelengths (inset: β-Ga_2O_3 bulk substrate).

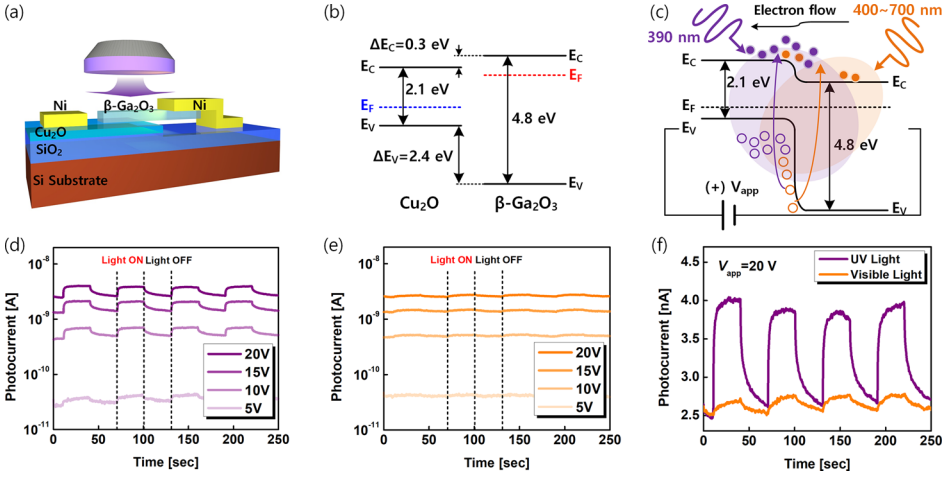

Figure 3. (a) Schematic view of the fabricated prototype Cu_2O/β-Ga_2O_3 pn heterojunction photodetector and time-dependent photoresponse measurement configuration. Energy band diagrams of the Cu_2O/β-Ga_2O_3 pn heterojunction photodetector: (b) before contact and (c) after contact under UV and visible lights. (d) Continuous time-dependent photoresponse characteristics in a forward mode of the Cu_2O/β-Ga_2O_3 pn heterojunction photodetector with various V_{app} conditions under UV light with a light intensity of 2.5 mW (λ = 390 nm) and (e) visible light with a light intensity of 10 W (λ = 400−700 nm). (f) Measured photoresponse characteristics under both UV and visible light at V_{app} = 20 V with a period of 30 s during turning the light on and off sequentially.

contact resistance to achieve a higher and better photosensitivity.

The composition and chemical state of the ALD-grown Cu_2O film surfaces were investigated via X-ray photoelectron spectroscopy (XPS) with a Kratos Axis Ultra DLD instrument. This is a surface-sensitive technique that can be used to analyze the surface chemical compositions of deposited films, as shown in Figure 2a,b. Figure 2a shows the survey scan XPS spectrum of the as-grown Cu_2O film with multiple peaks arising from Cu and O. The high-resolution XPS spectra in the vicinity of the Cu 2p peaks showed two distinct peaks at the binding energies of 932.2 and 951.1 eV, corresponding to the $2p_{3/2}$ and $2p_{1/2}$

DOI: 10.1021/acsomega.9b03149
ACS Omega 2019, 4, 20756−20761

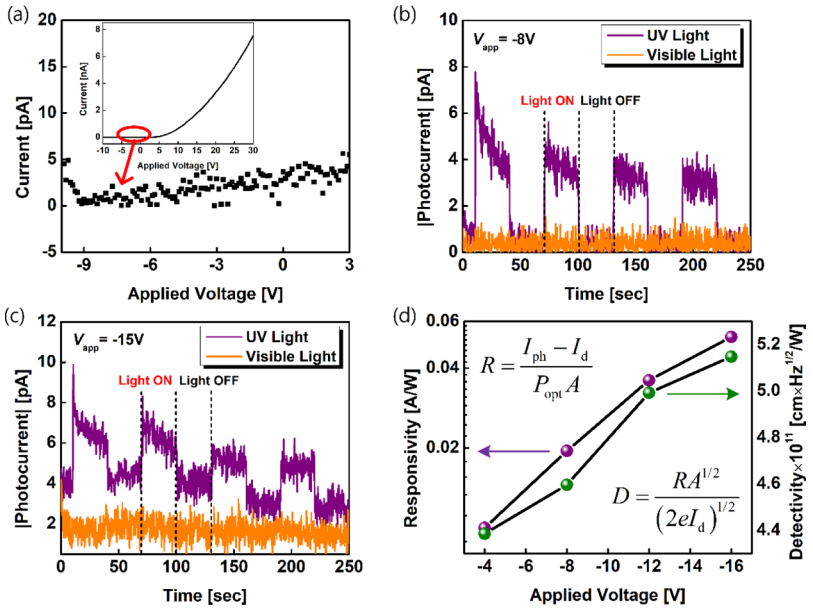

Figure 4. (a) Enlarged $I-V$ curve below zero V_{app}; the inset displays the measured $I-V$ data from −10 to +30 V. The dark current under the reverse mode of the V_{app}. Measured photoresponse characteristics as a function of time under the reverse mode of the Cu_2O/β-Ga_2O_3 pn heterojunction photodetector at (b) V_{app} = −5 V and (c) V_{app} = −15 V. (d) Both responsivity and detectivity of the Cu_2O/β-Ga_2O_3 pn heterojunction photodetector at various applied voltages under the reverse mode.

states of Cu^+ (Figure 2b). Two broad satellite peaks at 943−948 eV were also observed, both of which were attributed to the Cu^{2+} state (CuO) on the surface.[29] Clear evidence of the ALD-grown Cu_2O film is shown in Figure 2c through the scanning transmission electron microscopy (STEM) analysis and energy-dispersive X-ray spectroscopy (EDS) mapping images. The high-resolution atomic force microscopy (AFM) images of the surface morphologies of the Cu_2O film are shown in Figure 2d. The surface of the film was reasonably smooth with a roughness of approximately 4−5 nm. Figure 2e shows the ALD-grown Cu_2O thin film on the glass substrate. As shown in Figure 2f, the Cu_2O thin film with a thickness of 12 nm exhibited a high transparency of approximately 90%, resulting in light absorption below ∼500 nm, corresponding to an energy of approximately 2.4 eV.[30] The thickness of the β-Ga_2O_3 flake was measured by AFM, as illustrated in Figure 2g. The channel width was determined by the width of the flake because of the stochastic nature of the β-Ga_2O_3 exfoliation process. Figure 2h shows the transmittance characteristics of the β-Ga_2O_3 bulk sample used in the fabricated device. The inset of Figure 2h shows the optical image of the β-Ga_2O_3 bulk substrate. The optical transmission characteristics of both the Cu_2O and β-Ga_2O_3 films across the visible range of the spectrum is very high over 80%.[30]

Figure 3a shows a schematic view of the fabricated prototype p-type Cu_2O/n-type β-Ga_2O_3 pn heterojunction photodiode and the time-dependent photoresponse measurement configuration. To clearly illustrate the photoinduced electrical conduction mechanism, the energy band diagrams of the Cu_2O/β-Ga_2O_3 pn heterojunction are provided in Figure 3b,c. The band-gap energies of Cu_2O and β-Ga_2O_3 are 2.1 and 4.8 eV, respectively. The valence band offset (ΔE_V = 2.4 eV) and the conduction band offset (ΔE_C = 0.3 eV) of the Cu_2O/β-Ga_2O_3 pn heterojunction were calculated.[31] After being physically and electrically contacted, carriers can flow until both the Fermi levels align, and a pn heterojunction depletion layer formed near the interface of Cu_2O/β-Ga_2O_3. As shown in Figure 3c, when UV light irradiates the fabricated device, the light passes into the interface of the Cu_2O/β-Ga_2O_3 pn heterojunction and generates electron−hole pairs (ehp). In the fabricated device, the β-Ga_2O_3 film was doped with Sn at a concentration of 2.7 × 10^{18} cm^{-3}, so the separation of the photogenerated carriers by incident light is more effective and faster due to the larger conduction band offset.[32] When a positive (+) bias was applied to the Cu_2O side, electrons were transported toward the p-type Cu_2O. Both UV light with an intensity of 2.5 mW (λ = 390 nm) and visible light with an intensity of 10 W (λ = 400−700 nm) were used under the illumination of a fixed light intensity. The I_{ON}/I_{OFF} ratios with various applied voltages are described in Figure S5 of the Supporting Information. Figure 3d,e shows the photocurrent responses of the Cu_2O/β-Ga_2O_3 device under UV and visible light, respectively. Four repeat on−off cycles of the light source were used to examine the repeatability of the fabricated device under various applied voltages (V_{app}) from 5 to 20 V. Figure 3d,e shows the continuous time-dependent photoresponse characteristics in the forward mode of the Cu_2O/β-Ga_2O_3 device under various V_{app} conditions irradiated with UV and visible light, respectively. A switching period of 30 s was used for turning the light on and off sequentially. As shown in Figure 3f, the measured photocurrent drastically increases under UV light irradiation because the photogenerated carriers are significantly limited by visible light ranging from 400 to 700 nm.

Figure 4a shows the representative current−voltage characteristics under the reverse mode of the Cu_2O/β-Ga_2O_3 photodetector under various V_{app} conditions in the dark at room temperature (20 °C). The zero dark current is observed at an applied bias of approximately 8 V. As in previous measurements, when the photodetector is exposed to light, the induced photocurrent increases rapidly. In contrast, when the light is switched off, the light-induced photocurrent rapidly decreases. However, no photocurrent was generated by the visible light with a longer wavelength than that of UV light in

DOI: 10.1021/acsomega.9b03149
ACS Omega 2019, 4, 20756−20761

the two cases, as shown in Figure 4b,c. The induced photocurrent is directly attributed to the absorption of UV photons. The response and recovery time of the fabricated device under reverse biases are both estimated to be approximately 200 ms, as shown in Figure S6 of the Supporting Information. These fast response characteristics indicate that the fabricated Cu_2O/β-Ga_2O_3 pn heterostructure is promising for the detection of fast optical signals, with superior performance compared to that of previously developed oxide-based photodetector devices.[5] To quantitatively assess the device performance of the fabricated device, the responsivity (R) and detectivity (D) were calculated as shown in Figure 4d. The R and D at an applied voltage of −16 V were estimated to be 53 mA·W^{-1} and 5.2 × 10^{11} cm·Hz$^{1/2}$/W, respectively. In the two equations in the inset of Figure 4d, I_{ph} and I_d are the measured current under photonic and dark states, P_{opt} is the light intensity, A is the effective illuminated area (=8 × 10^{-5} cm^2), and e is the electric charge (=1.6 × 10^{-19} C). Meanwhile, although we investigated the characterization of a solar-blind UV photodetector using a single wavelength of 390 nm, comprehensive studies using the light source with a wide range of wavelengths is required for more practical applications as a further study.

CONCLUSIONS

We have successfully developed the thermal ALD process of p-type Cu_2O and integrated it with mechanically exfoliated n-type β-Ga_2O_3 as a hybrid pn heterojunction solar-blind UV photodetector. The p-type Cu_2O film is an important building block for all oxide-based electronic and photonic device research. In particular, the low temperature of the ALD process offers the unique opportunity to develop back-of-the-line transistor technology, even for mainstream Si-based CMOS applications. Inspired by the widely adopted two-dimensional van der Waals heterogeneous integration, this work provides a feasible route to integrate oxide-based pn heterojunctions for various device applications, which were previously limited by the challenging heterogeneous epitaxy techniques.

EXPERIMENTAL METHODS

Device Fabrication. The p-type Cu_2O thin film was deposited on 90 nm SiO_2/Si substrates by the ALD process with optimized conditions. The n-type β-Ga_2O_3 flakes were transferred onto the Cu_2O thin film by the exfoliation technique. Subsequently, Ni metal electrodes were formed by electron beam evaporation and lift-off process after photolithography patterning. The 6:1 HF solution was used not only to etch the Cu_2O film underneath the β-Ga_2O_3 flake but also to deposit each metal electrodes onto the p-type Cu_2O and n-type β-Ga_2O_3 flake, respectively.

Experimental Equipment. All electrical measurements were carried out in an ambient air environment without any device encapsulation. The electrical I−V characteristics were measured by using a B1500A semiconductor device analyzer. An AFM (model Veeco Dimension 3100) analysis was also conducted to assess the surface roughness of the atomic layer deposited Cu_2O film.

TEM Analysis. To confirm the well-deposited Cu_2O film layer, high-resolution TEM (FEI TALOS F200X operated at 200 kV) equipped with high angle annular dark field detectors and super X electron-dispersive X-ray spectroscopy was carried out.

XPS Analysis. The chemical composition of the Cu_2O film was investigated using the XPS system (Kratos Axis Ultra DLD) with monochromatic Al Kα radiation (1486.6 eV).

Transmittance Measurement. The transmittance of Cu_2O, β-Ga_2O_3, and the glass substrate was evaluated using Filmetrics F20 with a wavelength range from 380 to 1050 nm.

ASSOCIATED CONTENT

Supporting Information

The Supporting Information is available free of charge at https://pubs.acs.org/doi/10.1021/acsomega.9b03149.

Details about deposition of Cu_2O film by ALD with various growth temperatures, diagram of the ALD cycle for deposition of Cu_2O film, structural formula of the copper precursor, deposition rate of Cu_2O film at 180 °C, measured I−V curves of Cu_2O film with various contact metals, I_{ON}/I_{OFF} of the fabricated device under dark and photonic states, and response time according to the light on and off (PDF)

AUTHOR INFORMATION

Corresponding Author

*E-mail: yep@purdue.edu. Fax: 765-496-7443.

ORCID

Hagyoul Bae: 0000-0002-2462-4198
Mengwei Si: 0000-0003-0397-7741
Haiyan Wang: 0000-0002-7397-1209
Peide D. Ye: 0000-0001-8466-9745

Author Contributions

H.B. and P.D.Y. conceived the concept. H.B. developed this idea and designed overall research plans and methods. A.C. and D.Z. carried out the XPS analysis. H.B., J.N., M.S., and W.C. fabricated the devices. H.B., G.Q., X.L., and S.A. performed electrical measurements and data analysis. X.S. and H.W. contributed to the TEM and EDS characterizations. All authors discussed the experimental results and commented on the manuscript at all stages.

Notes

The authors declare no competing financial interest.

ACKNOWLEDGMENTS

This work was supported in part by ASCENT, one of six centers in JUMP, a Semiconductor Research Corporation Program through DARPA, in part by the Office of Naval Research's Naval Enterprise Partnership Teaming with Universities for National Excellence under grant N00014-15-1-2833. X.S. and H.W. acknowledge the support from the U.S. National Science Foundation for the TEM effort (DMR-1565822). H.B. was supported by a Fellowship from the National Research Foundation of Korea through the Ministry of Education under grant 2018R1A6A3A03013435.

REFERENCES

(1) Koppens, F. H. L.; Mueller, T.; Avouris, P.; Ferrari, A. C.; Vitiello, M. S.; Polini, M. Photodetectors based on Graphene, Other Two-Dimensional Materials and Hybrid Systems. *Nat. Nanotechnol.* **2014**, *9*, 780−793.

(2) Guo, Y.; Liu, C.; Tanaka, H.; Nakamura, E. Air-Stable and Solution-Processable Perovskite Photodetectors for Solar-Blind UV and Visible Light. *J. Phys. Chem. Lett.* **2015**, *6*, 535−539.

(3) Qin, J.-K.; Qiu, G.; He, W.; Jian, J.; Si, M. W.; Duan, Y. Q.; Charnas, A.; Zemlyanov, D. Y.; Wang, H. Y.; Shao, W. Z.; Zhen, L.;

DOI: 10.1021/acsomega.9b03149
ACS Omega 2019, 4, 20756−20761

Xu, C. Y.; Ye, P. D. Epitaxial Growth of 1D Atomic Chain Based Se Nanoplates on Monolayer ReS_2 for High-Performance Photodetectors. *Adv. Funct. Mater.* **2018**, *28*, 1806254.
(4) Kind, H.; Yan, H.; Messer, B.; Law, M.; Yang, P. Nanowire Ultraviolet Photodetectors and Optical Switches. *Adv. Mater.* **2002**, *14*, 158−160.
(5) Zhai, T.; Fang, X.; Liao, M.; Xu, X.; Zeng, H.; Yoshio, B.; Golberg, D. A Comprehensive Review of One-Dimensional Metal-Oxide Nanostructure Photodetectors. *Sensors* **2009**, *9*, 6504−6529.
(6) Li, A.; Chen, Q.; Wang, P.; Gan, Y.; Qi, T.; Wang, P.; Tang, F.; Wu, J. Z.; Chen, R.; Zhang, L.; Gong, Y. Ultrahigh-Sensitive Broadband Photodetectors Based on Dielectric Shielded $MoTe_2$/Graphene/SnS_2 p-g-n Junctions. *Adv. Mater.* **2018**, *31*, 1805656.
(7) Huang, M.; Wang, M.; Chen, C.; Ma, Z.; Li, X.; Han, J.; Wu, Y. Broadband Black-Phosphorus Photodetectors with High Responsivity. *Adv. Mater.* **2016**, *28*, 3481−3485.
(8) Pollack, G. P.; Trivich, D. Photoelectric Properties of Cuprous Oxide. *J. Appl. Phys.* **1975**, *46*, 163−172.
(9) Bai, Z.; Zhang, Y. Self-Powered UV-Visible Photodetectors based on ZnO/Cu_2O Nanowire/Electrolyte Heterojunctions. *J. Alloys Compd.* **2016**, *675*, 325−330.
(10) Liu, X.; Du, H.; Wang, P.; Lim, T.-T.; Sun, X. W. A High-Performance UV/Visible Photodetector of Cu_2O/ZnO Hybrid Nanofilms on SWNT-based Flexible Conducting Substrates. *J. Mater. Chem. C* **2014**, *2*, 9536−9542.
(11) Leskelä, M.; Ritala, M. Atomic Layer Deposition (ALD): from Precursors to Thin Film Structures. *Thin Solid Films* **2002**, *409*, 138−146.
(12) Waechtler, T.; Oswald, S.; Roth, N.; Jakob, A.; Lang, H.; Ecke, R.; Schulz, S. E.; Gessner, T.; Moskvinova, A.; Schulze, S.; Hietschold, M. Copper Oxide Films Grown by Atomic Layer Deposition from Bis(tri-*n*-butylphosphane)copper(I)acetylacetonate on Ta, TaN, Ru, and SiO_2. *J. Electrochem. Soc.* **2009**, *156*, H453−H459.
(13) Kim, S. K.; Choi, G.-J.; Lee, S. Y.; Seo, M.; Lee, S. W.; Han, J. H.; Ahn, H.-S.; Han, S.; Hwang, C. S. Al-Doped TiO_2 Films with Ultralow Leakage Currents for Next Generation DRAM Capacitors. *Adv. Mater.* **2008**, *20*, 1429−1435.
(14) Kim, H.; Lee, M. Y.; Kim, S.-H.; Bae, S. I.; Ko, K. Y.; Kim, H.; Kwon, K.-W.; Hwang, J.-H.; Lee, D.-J. Highly-Conformal p-Type Copper(I) Oxide (Cu_2O) Thin Films by Atomic Layer Deposition Using a Fluorine-Free Amino-Alkoxide Precursor. *Appl. Surf. Sci.* **2015**, *349*, 673−682.
(15) Kwon, J.-D.; Kwon, S.-H.; Jung, T.-H.; Nam, K.-S.; Chung, K.-B.; Kim, D.-H.; Park, J.-S. Controlled Growth and Properties of p-Type Cuprous Oxide Films by Plasma-Enhanced Atomic Layer Deposition at Low Temperature. *Appl. Surf. Sci.* **2013**, *285*, 373−379.
(16) Iivonen, T.; Heikkilä, M. J.; Popov, G.; Nieminen, H.-E.; Kaipio, M.; Kemell, M.; Mattinen, M.; Meinander, K.; Mizohata, K.; Räisänen, J.; Ritala, M.; Leskelä, M. Atomic Later Deposition of Photoconductive Cu_2O Thin Films. *ACS Omega* **2019**, *4*, 11205−11214.
(17) Shao, Z. G.; Chen, D. J.; Lu, H.; Zhang, R.; Cao, D. P.; Luo, W. J.; Zheng, Y. D.; Li, L.; Li, Z. H. High-Gain AlGaN Solar-Blind Avalanche Photodiodes. *IEEE Electron Device Lett.* **2014**, *35*, 372−374.
(18) Yu, J.; Shan, C. X.; Liu, J. S.; Zhang, X. W.; Li, B. H.; Shen, D. Z. MgZnO Avalanche Photodetectors Realized in Schottky Structures. *Phys. Status Solidi* **2013**, *7*, 425−428.
(19) Yang, W.; Hullavarad, S. S.; Nagaraj, B.; Takeuchi, I.; Sharma, R. P.; Venkatesan, T.; Vispute, R. D.; Shen, H. Compositionally-Tuned Epitaxial Cubic $Mg_xZn_{1-x}O$ on Si(100) for Deep Ultraviolet Photodetectors. *Appl. Phys. Lett.* **2003**, *82*, 3424−3426.
(20) Lee, Y. S.; Chua, D.; Brandt, R. E.; Siah, S. C.; Li, J. V.; Mailoa, J. P.; Lee, S. W.; Gordon, R. G.; Buonassisi, T. Atomic Layer Deposited Gallium Oxide Buffer Layer Enables 1.2 V Open-Circuit Voltage in Cuprous Oxide Solar Cells. *Adv. Mater.* **2014**, *26*, 4704−4710.
(21) Guo, D.; Wu, Z.; Li, P.; An, Y.; Liu, H.; Guo, X.; Yan, H.; Wang, G.; Sun, C.; Li, L.; Tang, W. Fabrication of β-Ga_2O_3 Thin Films and Solar-Blind Photodetectors by Laser MBE Technology. *Opt. Mater. Express* **2014**, *4*, 1067−1076.
(22) Qian, L. X.; Liu, X. Z.; Sheng, T.; Zhang, W. L.; Li, Y. R.; Lai, P. T. β-Ga_2O_3 Solar-Blind Deep-Ultraviolet Photodetector based on a Four-Terminal Structure with or without Zener Diodes. *AIP Adv.* **2016**, *6*, 045009.
(23) Orita, M.; Ohta, H.; Hirano, M.; Hosono, H. Deep-Ultraviolet Transparent Conductive β-Ga_2O_3 Thin Films. *Appl. Phys. Lett.* **2000**, *77*, 4166−4168.
(24) Pratiyush, A. S.; Krishnamoorthy, S.; Solanke, S. V.; Xia, Z.; Muralidharan, R.; Rajan, S.; Nath, D. N. High Responsivity in Molecular Beam Epitaxy Grown β-Ga_2O_3 Metal Semiconductor Metal Solar Blind Deep-UV Photodetector. *Appl. Phys. Lett.* **2017**, *110*, 221107.
(25) Oshima, T.; Okuno, T.; Arai, N.; Suzuki, N.; Ohira, S.; Fujita, S. Vertical Solar-Blind Deep-Ultraviolet Schottky Photodetectors Based on β-Ga_2O_3 Substrates. *Appl. Phys. Express* **2008**, *1*, 011202.
(26) Galazka, Z.; Irmscher, K.; Uecker, R.; Bertram, R.; Pietsch, M.; Kwasniewski, A.; Naumann, M.; Schulz, T.; Schewski, R.; Klimm, D.; Bickermann, M. On the Bulk β-Ga_2O_3 Single Crystals Grown by the Czochralski Method. *J. Cryst. Growth* **2014**, *404*, 184−191.
(27) Higashiwaki, M.; Sasaki, K.; Murakami, H.; Kumagai, Y.; Koukitu, A.; Kuramata, A.; Masui, T.; Yamakoshi, S. Recent Progress in Ga_2O_3 Power Devices. *Semicond. Sci. Technol.* **2016**, *31*, 034001.
(28) Lim, B. S.; Rahtu, A.; Gordon, R. G. Atomic Layer Deposition of Transition Metals. *Nat. Mater.* **2003**, *2*, 749−754.
(29) Ghijsen, J.; Tjeng, L. H.; van Elp, J.; Eskes, H.; Westerink, J.; Sawatzky, G. A.; Czyzyk, M. T. Electronic Structure of Cu_2O and CuO. *Phys. Rev. B: Condens. Matter Mater. Phys.* **1988**, *38*, 11322.
(30) Mi, W.; Ma, J.; Luan, C.; Xiao, H. Structural and Optical Properties of β-Ga_2O_3 films Deposited on $MgAl_2O_4$(100) Substrates by Metal-Organic Chemical Vapor Deposition. *J. Lumin.* **2014**, *146*, 1−5.
(31) Watahiki, T.; Yuda, Y.; Furukawa, A.; Yamamuka, M.; Takiguchi, Y.; Miyajima, S. Heterojunction p-Cu_2O/n-Ga_2O_3 Diode with High Breakdown Voltage. *Appl. Phys. Lett.* **2017**, *111*, 222104.
(32) Guo, D.; Su, Y.; Shi, H.; Li, P.; Zhao, N.; Ye, J.; Wang, S.; Liu, A.; Chen, Z.; Li, C.; Tang, W. Self-Powered Ultraviolet Photodetector with Superhigh Photoresponsivity (3.05 A/W) Based on the GaN/Sn:Ga_2O_3 pn Junction. *ACS Nano* **2018**, *12*, 12827−12835.

DOI: 10.1021/acsomega.9b03149
ACS Omega 2019, 4, 20756−20761